Journal of Biomechanics ▮ (▮▮▮▮) ▮▮▮–▮▮▮

Contents lists available at ScienceDirect

Journal of Biomechanics

journal homepage: www.elsevier.com/locate/jbiomech
www.JBiomech.com

Short communication

Influence of joint constraints on lower limb kinematics estimation from skin markers using global optimization

Sonia Duprey [a,b,c,*], Laurence Cheze [a,b,c], Raphaël Dumas [a,b,c]

[a] Université de Lyon, F-69622 Lyon, France
[b] INRETS, UMR_T9406, Laboratoire de Biomécanique et Mécanique des Chocs, F-69625 Bron, France
[c] Université Lyon 1, Villeurbanne, France

ARTICLE INFO

Article history:
Accepted 3 June 2010

Keywords:
Soft tissue artefact
Lower limb
Kinematics
Gait analysis
Optimization

ABSTRACT

In order to obtain the lower limb kinematics from skin-based markers, the soft tissue artefact (STA) has to be compensated. Global optimization (GO) methods rely on a predefined kinematic model and attempt to limit STA by minimizing the differences between model predicted and skin-based marker positions. Thus, the reliability of GO methods depends directly on the chosen model, whose influence is not well known yet.

This study develops a GO method that allows to easily implement different sets of joint constraints in order to assess their influence on the lower limb kinematics during gait. The segment definition was based on generalized coordinates giving only linear or quadratic joint constraints. Seven sets of joint constraints were assessed, corresponding to different kinematic models at the ankle, knee and hip: SSS, USS, PSS, SHS, SPS, UHS and PPS (where S, U and H stand for spherical, universal and hinge joints and P for parallel mechanism). GO was applied to gait data from five healthy males.

Results showed that the lower limb kinematics, except hip kinematics, knee and ankle flexion–extension, significantly depend on the chosen ankle and knee constraints. The knee parallel mechanism generated some typical knee rotation patterns previously observed in lower limb kinematic studies. Furthermore, only the parallel mechanisms produced joint displacements.

Thus, GO using parallel mechanism seems promising. It also offers some perspectives of subject-specific joint constraints.

1. Introduction

To obtain an accurate skeleton kinematics from skin-based markers, the relative motion of soft tissues with regards to the underlying bone (i.e., the soft tissue artefact (STA)) has to be compensated. Several methods minimizing STA have been developed (Leardini et al., 2005). Some methods address each segment separately by computing the optimal bone pose from a marker cluster (Söderkvist and Wedin, 1993; Challis, 1995; Cheze et al., 1995), while global optimization (GO) methods address the entire limb, or full body, by minimizing distances between measured and model-determined marker positions (Lu and O'Connor, 1999). GO methods rely on the determination of a predefined kinematic model with specific joint constraints. Therefore, GO results directly depend on the constraint choices.

Spherical joints have been classically applied (Lu and O'Connor, 1999; Charlton et al., 2004). Alternatively, models including universal and hinge joints at the ankle and knee were proposed (Reinbolt et al., 2005; Andersen et al., 2009). Moreover, degree-of-freedom coupling curves were included as knee joint constraints in a registration technique (Sholukha et al., 2006) providing reliable results in terms of joint displacements. However the coupling curves were dependent on the chosen segment axes and Euler angle sequence.

Coupled degrees-of-freedom can also be modelled by spatial parallel mechanisms (Feikes et al., 2003; Di Gregorio et al., 2007) that directly take into account anatomical structures (i.e., articular surfaces as sphere-on-plane contacts and ligaments as constant lengths). The corresponding joint constraints have not been included in GO methods so far.

The aim of the current study is to develop a GO method that allows to easily implement different sets of joint constraints, in order to assess their influence on the lower limb kinematics during gait. Different sets of joint constraints were evaluated, corresponding to different kinematic models at the ankle, knee and hip joints: SSS, USS, PSS, SHS, SPS, UHS and PPS (where S, U and H stand for spherical, universal and hinge joints and P for parallel mechanism).

* Corresponding author at: LBMC, INRETS, 25 Av. F Mitterrand, F-69675 Bron Cedex, France. Tel.: +33 4 78 65 68 82; fax: +33 4 72 14 23 60.
E-mail address: sonia.duprey@univ-lyon1.fr (S. Duprey).

0021-9290/$ - see front matter © 2010 Elsevier Ltd. All rights reserved.
doi:10.1016/j.jbiomech.2010.06.010

2. Global optimization methods (see Appendices A–C for more details)

2.1. Parameter set

GO was performed using generalized coordinates (Dumas and Cheze, 2007) consisting, for each segment i, of two position vectors (the proximal P_i and distal D_i endpoints) and two unitary direction vectors ($\mathbf{u}_i$ and $\mathbf{w}_i$):

$$\mathbf{Q}_i = \begin{bmatrix} \mathbf{u}_i & \mathbf{r}_{P_i} & \mathbf{r}_{D_i} & \mathbf{w}_i \end{bmatrix}^T \quad (1)$$

with $i=1$, 2, 3 and 4 for the foot, shank, thigh and pelvis, respectively.

These parameters were designed to stand for non-orthogonal directions: inertial (for inverse dynamics purpose), anatomical (i.e., from joint centre to joint centre) and functional (i.e., mean axis of rotation). Particularly, r_{D_2} and r_{P_2} are the ankle and knee joint centres while $\mathbf{w}_2$ and $\mathbf{w}_3$ are the ankle and knee flexion–extension axes. In addition, any position $\mathbf{r}$ of a point (marker or virtual) and any direction $\mathbf{n}$ embedded in the segment i can be straightforwardly deduced from $\mathbf{Q}_i$ through a constant interpolation matrix $\mathbf{N}_i$ (Garcia de Jalon et al., 1986; Dumas and Cheze, 2007). As 12 parameters represent the 6 degrees-of-freedom of the segment, rigid body constraints have to be considered in addition to the joint constraints.

2.2. Objective function

The objective function to minimize is the sum of the square distances between measured and model-determined marker positions:

$$f = \sum_{i=1}^{4} \sum_{j=1}^{m_i} (\mathbf{r}_{M_i^j} - \mathbf{N}_i^{M_i^j} \mathbf{Q}_i)^2 \quad (2)$$

with M_i^j is the jth marker (out of m_i) embedded in segment i, $\mathbf{r}_{M_i^j}$ its measured position and $\mathbf{N}_i^{M_i^j}$ the corresponding interpolation matrix.

2.3. Joint constraints

For the spherical model, the joint constraints at the ankle, knee and hip are

$$\mathbf{r}_{D_{i+1}} - \mathbf{r}_{P_i} = 0 \quad (i=1{:}2) \quad \text{and} \quad \mathbf{N}_4^{V_4^1} \mathbf{Q}_4 - \mathbf{r}_{P_3} = 0 \quad (3)$$

with V_4^1 a virtual point (i.e., hip joint centre) embedded in the pelvis segment and $\mathbf{N}_4^{V_4^1}$ the corresponding interpolation matrix.

For the universal joint at the ankle, the joint constraints are

$$\begin{cases} \mathbf{r}_{D_2} - \mathbf{r}_{P_1} = 0 \\ \mathbf{w}_2 \cdot \mathbf{N}_1^{\mathbf{n}_1^1} \mathbf{Q}_1 - \cos\theta_A = 0 \end{cases}, \quad (4)$$

with θ_A the angle defining the relative orientation of the two functional joint axes, $\mathbf{n}_1^1$ an axis (i.e., subtalar) embedded in the foot segment and $\mathbf{N}_1^{\mathbf{n}_1^1}$ the corresponding interpolation matrix.

For the hinge model at the knee, the joint constraints are

$$\begin{cases} \mathbf{r}_{D_3} - \mathbf{r}_{P_2} = 0 \\ \mathbf{w}_3 \cdot (\mathbf{r}_{P_2} - \mathbf{r}_{D_2}) - L_2 \cos\theta_K^1 = 0 \\ \mathbf{w}_3 \cdot \mathbf{u}_2 - \cos\theta_K^2 = 0 \end{cases} \quad (5)$$

with θ_K^1 and θ_K^2 two angles defining the orientation of the joint axes and L_2 the shank segment length.

For the parallel mechanism at the ankle (Di Gregorio et al., 2007), the joint constraints are

$$\begin{cases} (\mathbf{N}_1^{V_1^1} \mathbf{Q}_1 - \mathbf{N}_2^{V_2^1} \mathbf{Q}_2) \cdot \mathbf{N}_2^{\mathbf{n}_2^1} \mathbf{Q}_2 - d_A^1 = 0 \\ (\mathbf{N}_1^{V_1^2} \mathbf{Q}_1 - \mathbf{N}_2^{V_2^2} \mathbf{Q}_2) \cdot \mathbf{N}_2^{\mathbf{n}_2^2} \mathbf{Q}_2 - d_A^2 = 0 \\ (\mathbf{N}_2^{V_2^3} \mathbf{Q}_2 - \mathbf{N}_1^{V_1^3} \mathbf{Q}_1)^2 - (d_A^3)^2 = 0 \\ (\mathbf{N}_2^{V_2^4} \mathbf{Q}_2 - \mathbf{N}_1^{V_1^4} \mathbf{Q}_1)^2 - (d_A^4)^2 = 0 \\ (\mathbf{N}_1^{V_1^5} \mathbf{Q}_2 - \mathbf{N}_1^{V_1^5} \mathbf{Q}_2) \cdot \mathbf{N}_1^{\mathbf{n}_1^2} \mathbf{Q}_1 - d_A^5 = 0 \end{cases} \quad (6)$$

These constraints represent the tibia/talus sphere-on-plane medial and lateral contacts (sphere centres V_1^1, V_1^2 and radii d_A^1, d_A^2, contact plane points V_2^1, V_2^2 and normals $\mathbf{n}_2^1$, $\mathbf{n}_2^2$), the calcaneum–tibia, calcaneum–fibula ligaments (origins V_2^3, V_2^4; insertions V_1^3, V_1^4 and lengths d_A^3, d_A^4) and the fibula/talus sphere-on-plane contact (centre V_2^5 and radius d_A^5, contact plane point V_1^5 and normal $\mathbf{n}_1^2$).

For the parallel mechanism at the knee (Feikes et al., 2003), the joint constraints are

$$\begin{cases} (\mathbf{N}_3^{V_3^1} \mathbf{Q}_3 - \mathbf{N}_2^{V_2^6} \mathbf{Q}_2) \cdot \mathbf{N}_2^{\mathbf{n}_2^3} \mathbf{Q}_2 - d_K^1 = 0 \\ (\mathbf{N}_3^{V_3^2} \mathbf{Q}_3 - \mathbf{N}_2^{V_2^7} \mathbf{Q}_2) \cdot \mathbf{N}_2^{\mathbf{n}_2^4} \mathbf{Q}_2 - d_K^2 = 0 \\ (\mathbf{N}_3^{V_3^3} \mathbf{Q}_3 - \mathbf{N}_2^{V_2^8} \mathbf{Q}_2)^2 - (d_K^3)^2 = 0 \\ (\mathbf{N}_3^{V_3^4} \mathbf{Q}_3 - \mathbf{N}_2^{V_2^9} \mathbf{Q}_2)^2 - (d_K^4)^2 = 0 \\ (\mathbf{N}_3^{V_3^5} \mathbf{Q}_3 - \mathbf{N}_2^{V_2^{10}} \mathbf{Q}_2)^2 - (d_K^5)^2 = 0 \end{cases} \quad (7)$$

These constraints represent the femur/tibia sphere-on-plane medial and lateral contacts (sphere centres V_3^1, V_3^2; radii d_K^1, d_K^2; contact plane points V_2^6, V_2^7 and normals $\mathbf{n}_2^3$, $\mathbf{n}_2^4$) and the anterior cruciate, posterior cruciate and medial collateral ligaments (origins V_3^3, V_3^4, V_3^5; insertions V_2^8, V_2^9, V_2^{10} and lengths d_K^3, d_K^4, d_K^5).

2.4. Model construction and initial guess

The construction of the lower limb kinematic models corresponds to the determination of the constants (i.e., interpolation matrices $\mathbf{N}$, angles θ, lengths L and distances d) from static calibration, functional methods and literature data (Di Gregorio et al., 2007; Feikes et al., 2003).

In the optimization process, the initial values of the parameters are obtained by constructing at each frame the position vectors $\mathbf{r}_{P_i}$ and $\mathbf{r}_{D_i}$ and direction vectors $\mathbf{u}_i$ and $\mathbf{w}_i$ from the skin-based markers (Dumas and Cheze, 2007; see also Appendix A).

2.5. Application

Five healthy male subjects (age: 28.8 ± 4.8 years; height: 1.74 ± 0.09 m; mass: 76.5 ± 13.5 kg) participated in this study. The trajectories of 32 skin-based markers on the right lower limb were recorded at 100 Hz. The parameters $\mathbf{Q}_i$ were obtained by minimization of the objective function f under constraints (i.e., rigid body and different sets of kinematic constraints) with the use of the "*fmincon*" Matlab function (Mathworks, USA). Then, the classical segment coordinate systems were deduced from the $\mathbf{Q}_i$ parameters (Dumas and Cheze, 2007) and the joint angles and displacements were computed (Wu et al., 2002; see also Appendix C). RMS differences were computed for each curve and averaged for the 5 subjects.

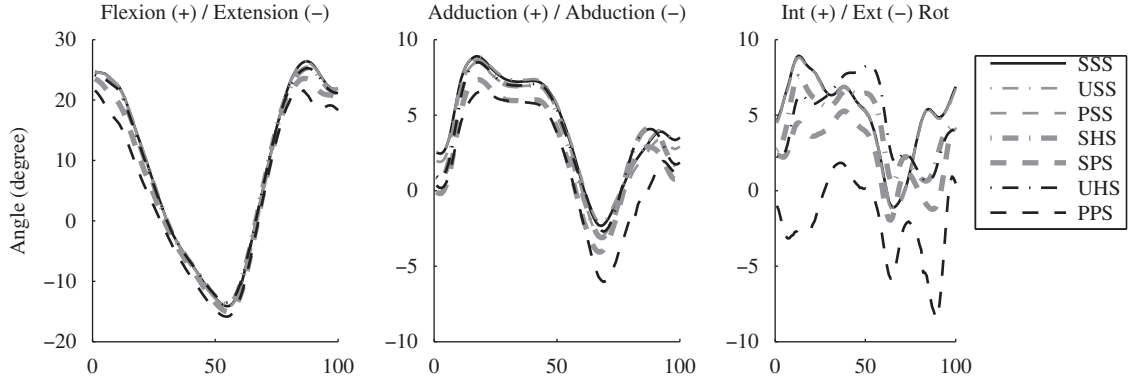

Fig. 1. Hip rotations for the SSS, USS, PSS, SHS, SPS, UHS and PPS kinematic constraints versus percentage of gait cycle for Subject 5.

Please cite this article as: Duprey, S., et al., Influence of joint constraints on lower limb kinematics estimation from skin markers using global optimization. Journal of Biomechanics (2010), doi:10.1016/j.jbiomech.2010.06.010

3. Results

3.1. Constraint influence

The hip kinematics was not much affected by ankle and knee constraint variations (Fig. 1, Table 1): all models provided similar patterns and amplitudes for the hip flexion–extension and abduction–adduction and the dispersion of the internal–external rotations remained low.

The knee flexion–extension curves did not vary across models: a single pattern could be observed and the dispersion was low. The patterns of the abduction–adduction, internal–external rotation and displacement curves appeared to depend on the applied knee constraint (Fig. 2) but not on the ankle constraint. However, ankle constraints caused a dispersion of the internal–external rotations (Table 1).

The ankle flexion–extension curves showed a similar pattern for all models with a slight dispersion (Fig. 3). The ankle abduction–adduction, internal–external rotation and displacement curves varied whenever the ankle or knee constraint was modified (Tables 1 and 2), except for the PPS and PSS models which provided similar rotation patterns and, for some subjects, similar displacement patterns.

Table 1
RMS differences between joint rotations in degree—average of the 5 subjects (FE, AA and IER stand for flexion–extension, abduction–adduction and internal–external rotations).

RMS difference	Hip			Knee			Ankle		
	FE	AA	IER	FE	AA	IER	FE	AA	IER
USS–SSS	0.09	0.09	0.04	0.07	0.10	1.29	0.18	1.01	2.19
PSS–SSS	0.36	0.48	0.28	0.36	1.26	5.06	3.13	9.50	9.01
USS–PSS	0.37	0.52	0.29	0.36	1.31	5.42	3.13	9.98	9.79
SPS–PPS	2.24	1.84	4.82	1.57	0.01	1.03	4.85	10.61	18.30
SHS–SSS	1.05	1.99	3.13	0.38	3.63	6.45	1.53	2.85	4.60
SPS–SSS	3.00	1.90	5.33	1.68	3.57	16.59	3.05	3.44	12.45
SHS–SPS	2.06	1.06	2.85	1.45	1.26	12.38	3.22	2.86	10.10
PSS–PPS	5.33	2.50	9.98	3.26	3.48	19.76	4.16	2.76	2.03
UHS–SSS	1.35	1.92	4.46	0.40	3.63	7.30	1.54	3.67	2.20
PPS–SSS	5.18	2.77	9.98	3.12	3.57	16.00	5.06	11.25	7.36
UHS–PPS	3.94	2.42	6.49	2.86	1.26	10.51	5.15	10.75	8.38
PSS–SPS	3.15	1.80	5.33	1.83	3.49	20.44	2.24	9.19	20.03
Average	**2.34**	**1.61**	**4.41**	**1.45**	**2.21**	**10.19**	**3.10**	**6.49**	**8.87**

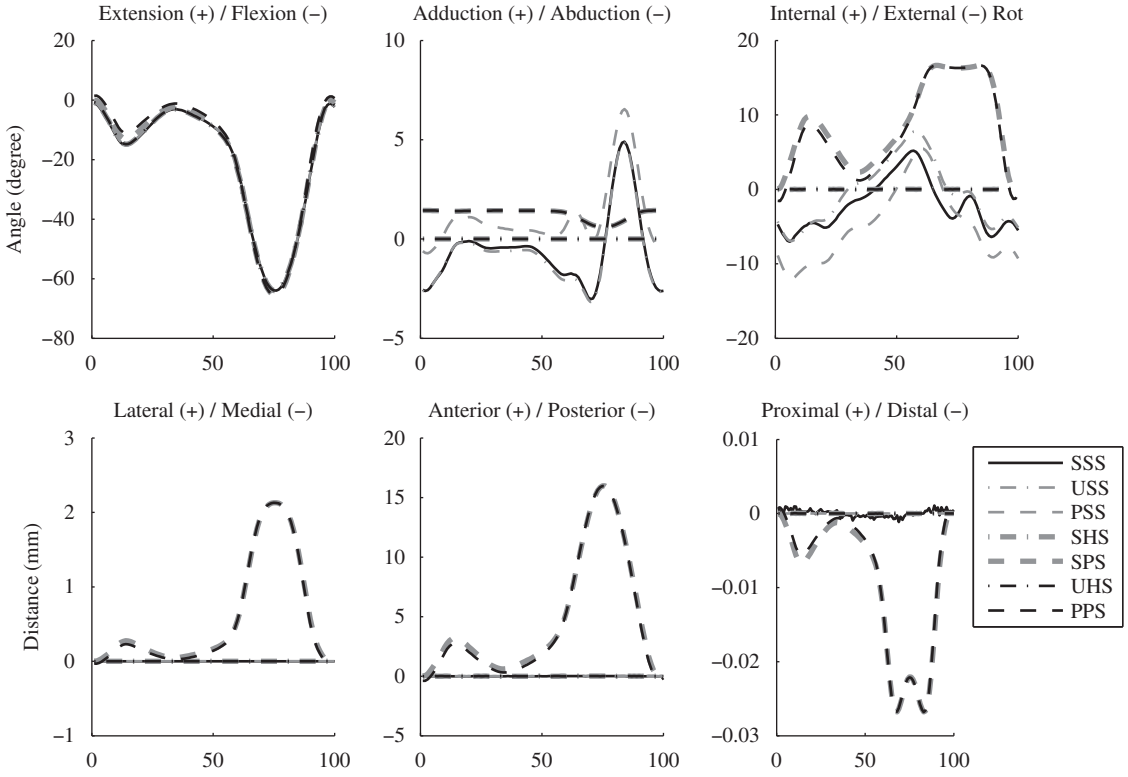

Fig. 2. Knee rotations and displacements for the SSS, USS, PSS, SHS, SPS, UHS and PPS kinematic constraints versus percentage of gait cycle for Subject 5.

Please cite this article as: Duprey, S., et al., Influence of joint constraints on lower limb kinematics estimation from skin markers using global optimization. Journal of Biomechanics (2010), doi:10.1016/j.jbiomech.2010.06.010

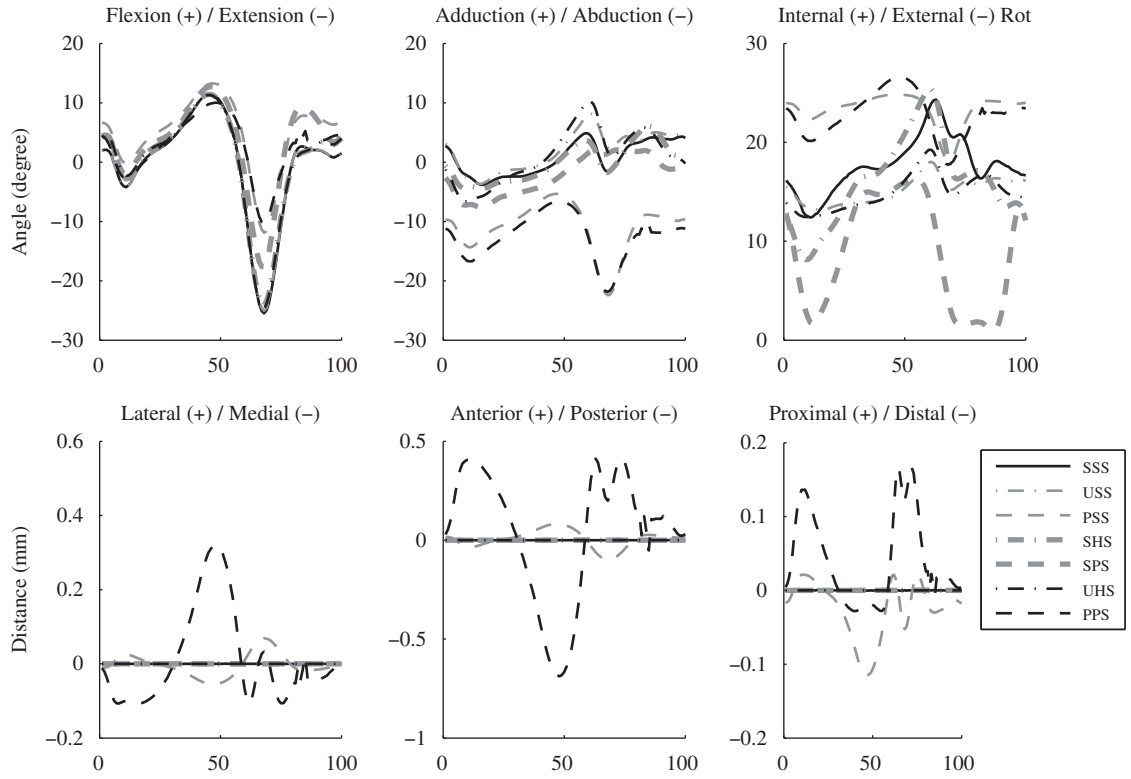

Fig. 3. Ankle rotations and displacements for the SSS, USS, PSS, SHS, SPS, UHS and PPS kinematic constraints versus percentage of gait cycle for Subject 5.

Table 2
RMS differences between joint displacements in millimetres—average of the 5 subjects (LM, AP and PD stand for lateral–medial, antero-posterior and proximal–distal displacements).

RMS difference	Knee			Ankle		
	LM	AP	PD	LM	AP	PD
USS–SSS	0.00	0.00	0.00	0.00	0.00	0.00
PSS–SSS	0.00	0.00	0.00	0.05	0.17	0.06
USS–PSS	0.00	0.00	0.00	0.05	0.17	0.06
SPS–PPS	0.04	0.38	0.00	0.08	0.32	0.09
SHS–SSS	0.00	0.00	0.00	0.00	0.00	0.00
SPS–SSS	0.97	6.72	0.01	0.00	0.00	0.00
SHS – SPS	0.97	6.72	0.01	0.00	0.00	0.00
PSS–PPS	0.95	6.58	0.01	0.09	0.34	0.08
UHS – SSS	0.00	0.00	0.00	0.00	0.00	0.00
PPS–SSS	0.95	6.58	0.01	0.08	0.32	0.09
UHS – PPS	0.95	6.58	0.01	0.08	0.32	0.09
PSS–SPS	0.97	6.72	0.01	0.05	0.17	0.06
Average	**0.48**	**3.36**	**0.01**	**0.04**	**0.15**	**0.05**

3.2. Comparison with in-vivo (intra-cortical pins) data from the literature

The hip kinematics reproduced typical patterns (the authors were not aware of any hip *in-vivo* data).

The knee flexion–extension biphasic pattern (Lafortune et al., 1992; Benoit et al., 2006; Andersen et al., 2010) was obtained for all models. Abduction–adduction of limited amplitude and internal rotation occurring twice during the stance phase (at heel strike and toe-off) were found when the model included a knee parallel mechanism. Furthermore, only the knee parallel mechanism could reproduce the femoral rollback.

The ankle flexion–extension curves reproduced the typical 2-peak pattern (Reinschmidt, 1996; Reinschmidt et al., 1997). All models roughly produced an initial abduction followed by a slight adduction during stance and internal–external rotations of limited amplitude, as observed in *in-vivo* studies (Reinschmidt, 1996; Reinschmidt et al., 1997). Besides, only the parallel mechanisms produced joint displacements.

4. Discussion and conclusions

GO with joint constraints is one of the methods developed for minimizing STA. Its reliability is under controversy (Stagni et al., 2009; Andersen et al., 2010). Nevertheless, defining a kinematic model is becoming usual in gait analysis (e.g., inverse–forward dynamics, musculoskeletal models, etc.) and the constraint choice is essential.

Please cite this article as: Duprey, S., et al., Influence of joint constraints on lower limb kinematics estimation from skin markers using global optimization. Journal of Biomechanics (2010), doi:10.1016/j.jbiomech.2010.06.010

In this study, a GO method was developed to implement different sets of joint constraints. The segment definition, based on generalized coordinates (Dumas and Cheze, 2007), allowed to readily implement complex constraints. Besides, the classical segment and joint coordinate systems could easily be deduced.

Results showed that the lower limb kinematics, except hip kinematics, knee and ankle flexion–extension, significantly depend on the chosen set of constraints. An appropriate choice, such as the parallel mechanisms, seemed to provide physiologic patterns (i.e., limited abduction–adduction at the knee and femoral rollback). Furthermore, these mechanisms offer the possibility of matching model geometry with MRI data (e.g., by customizing the femur condyles centre and radius) and adapting the model to pathologies (e.g., by suppressing a ligament constraint). Thus, these mechanisms might be able to provide efficient subject-specific models for clinical applications.

A major limitation of this study is the lack of *in-vivo* data. The ability to reproduce inter-subject variability, which is an important criterion in the constraint choice, could not be assessed and subject-by-subject validation could not be performed. Thus, further studies enabling subject-by-subject comparisons would offer interesting perspectives.

Conflict of interest statement

The authors hereby affirm that the study entitled "Influence of joint constraints on lower limb kinematics estimation from skin markers using global optimization" does not raise any conflict of interest. The opinions expressed in this paper are the opinions of the authors alone.

Appendix A. Supporting information

Supplementary data associated with this article can be found in the online version at doi:10.1016/j.jbiomech.2010.06.010.

References

Andersen, M.S., Benoit, D.L., Damsgaard, M., Ramsey, D.K., Rasmussen, J., 2010. Do kinematic models reduce the effects of soft tissue artefacts in skin marker-based motion analysis? An *in vivo* study of knee kinematics. J. Biomech. 43 (2), 268–273.

Andersen, M.S., Damsgaard, M., Rasmussen, J., 2009. Kinematic analysis of over-determinate biomechanical systems. Comput. Methods Biomech. Biomed. Eng. 12 (4), 371–384.

Benoit, D.L., Ramsey, D.K., Lamontagne, M., Xu, L., Wretenberg, P., Renström, P., 2006. Effect of skin movement artifact on knee kinematics during gait and cutting motions measured *in vivo*. Gait Posture 24, 152–164.

Challis, J.H., 1995. A procedure for determining rigid body transformation parameters. J. Biomech. 28 (6), 733–737.

Charlton, I.W., Tate, P., Smyth, P., Roren, L., 2004. Repeatability of an optimised lower body model. Gait Posture 20, 213–221.

Cheze, L., Fregly, B.J., Dimnet, J., 1995. A solidification procedure to facilitate kinematic analyses based on video system data. J. Biomech. 28 (7), 879–884.

Di Gregorio, R., Parenti-Castelli, V., O'Connor, J.J., Leardini, A., 2007. Mathematical models of passive motion at the human ankle joint by equivalent spatial parallel mechanisms. Med. Bio. Eng. Comput. 45, 305–313.

Dumas, R., Cheze, L., 2007. 3D inverse dynamics in non-orthonormal segment coordinate system. Med. Bio. Eng. Comput. 45, 315–322.

Feikes, J.D., O'Connor, J.J., Zavatsky, A.B., 2003. A constraint-based approach to modelling the mobility of the human knee joint. J. Biomech. 36 (1), 125–129.

Garcia de Jalon, J., Unda, J., Avello, A., 1986. Natural coordinates for the computer analysis of multibody systems. Comput. Meth. Appl. Mech. Eng. 56, 309–327.

Lafortune, M.A., Cavanagh, P.R., Sommer III, H.J., Kalenak, A., 1992. Three-dimensional kinematics of the human knee during walking. J. Biomech. 25 (4), 347–357.

Leardini, A., Chiari, L., Della Croce, U., Cappozzo, A., 2005. Human movement analysis using stereophotogrammetry. Part 3: soft tissue artifact assessment and compensation. Gait Posture 21, 212–225.

Lu, T.-W., O'Connor, J.J., 1999. Bone position estimation from skin marker co-ordinates using global optimisation with joint constraints. J. Biomech. 32 (2), 129–134.

Reinbolt, J.A., Schutte, J.F., Fregly, B.J., Koh, B.I., Haftkab, R.T., George, A.D., Mitchell, K.H., 2005. Determination of patient-specific multi-joint kinematic models through two-level optimization. J. Biomech. 38 (3), 621–626.

Reinschmidt, C., 1996. Three-dimensional tibiocalcaneal and tibiofemoral kinematics during human locomotion—measured with external and bone markers. Ph.D. Report. University of Calgary, Alberta, Canada.

Reinschmidt, C., van den Bogert, A.J., Murphy, N., Lundberg, A., Nigg, B.M., 1997. Tibiocalcaneal motion during running, measured with external and bone markers. Clinical Biomech. 12 (1), 8–16.

Sholukha, V., Leardini, A., Salvia, P., Rooze, M., Van Sint Jan, S., 2006. Double-step registration of *in vivo* stereophotogrammetry with both *in vitro* 6-DOFs electrogoniometry and CT medical imaging. J. Biomech. 39 (11), 2087–2095.

Söderkvist, I., Wedin, P.A., 1993. Determining the movements of the skeleton using well-configured markers. J. Biomech. 26 (12), 1473–1477.

Stagni, R., Fantozzi, S., Cappello, A., 2009. Double calibration vs. global optimisation: performance and effectiveness for clinical application. Gait Posture 29, 119–122.

Wu, G., van der Helm, F.C.T., Veeger, H.E.J., Makhsous, M., Van Roy, P., Anglin, C., Nagels, J., Karduna, A.R., McQuade, K., Wang, X., Werner, F.W., Buccholz, B., 2002. ISB recommendation on definitions of joint coordinate system of various joints for the reporting of human joint motion—part I: ankle, hip, and spine. J. Biomech. 38 (5), 981–992.

Please cite this article as: Duprey, S., et al., Influence of joint constraints on lower limb kinematics estimation from skin markers using global optimization. Journal of Biomechanics (2010), doi:10.1016/j.jbiomech.2010.06.010